CHARACTERISTICS OF LAMINAR AND TURBULENT ARGON PLASMA JETS IMPINGING NORMALLY UPON A WORKPIECE IN AMBIENT AIR

Hai-Xing Wang[1], Kai Cheng[2], Xi Chen[3] and Wenxia Pan[4]

[1] School of Astronautics, Beijing University of Aeronautics and Astronautics, Beijing 100083, China
[2] Shanghai Turbine Co. Ltd., 333 Jiangchuan Road, Minhang, Shanghai 200240, China.
[3] Department of Engineering Mechanics, Tsinghua University, Beijing 100084, China.
[4] Institue of Mechanics, Chinese Academy of Sciences, Beijing 100080, China.
whx@buaa.edu.cn, cx-dem@mail.tsinghua.edu.cn

ABSTRACT

Modeling results are presented concerning the characteristics of laminar and turbulent argon plasma jets impinging normally upon a flat plate (workpiece) in ambient air. It is found that the presence of the flat plate significantly enhances the entrainment rate of ambient air into the jets and affects on the flow and temperature fields in the near-plate region of the jets. At comparatively large distances between the plate and the jet inlet, the axial gradients of the plasma parameters in the laminar plasma impinging-jets assume values much less than those in the turbulent plasma impinging-jets.

INTRODUCTION

Turbulent thermal plasma jets have been extensively employed in industry and in labs for materials processing, such as in plasma spraying, plasma remelting, plasma waste treatment, etc. Usually turbulent plasma jets are accompanied by large flow fluctuations, intensive noise emission, strong entrainment of ambient gas into the plasma jets and thus with shorter high-temperature region lengths and steep axial gradients of plasma parameters (temperature, axial velocity, etc.). These special features of the turbulent plasma jets are often not favorable from the viewpoint of materials processing, because they will worsen the working surroundings of operators, reduce the process repeatability and controllability, and increase the oxidization degree of metallic materials processed in air surroundings.

With a specially designed DC non-transferred arc plasma torch, both long laminar and short turbulent plasma jets can be generated in experiments [1]. The long laminar plasma jet has a few attractive merits, including its stable flow state, low noise emission, low ambient-air entrainment rate, adjustable jet flow-field characteristics, etc. Preliminary attempts to use the laminar plasma jet in materials processing, including the re-melting or cladding hardening of metallic surfaces and the preparation of thermal barrier coating, have shown encouraging results [1, 2]. In order to deepen our understanding on the laminar plasma jet and promote its applications, Ref. [3] compared the characteristics of laminar and turbulent argon plasma jets issuing freely into ambient air. As a continuation of [3], this paper compares the characteristics for the laminar and turbulent argon plasma jets impinging normally upon a flat workpiece located in ambient air.

MODELING APPROACH

The main assumptions employed in this study include (i) the jet flow is steady and axi-symmetrical; (ii) the plasma is in the local thermodynamic equilibrium (LTE) state and optically thin to radiation; (iii) the swirling velocity is negligible compared with the axial velocity; (iv) the diffusion of argon within the argon-air mixture can be handled by the combined-diffusion-coefficient method [3-6] for the laminar case and by the turbulence-enhanced combined-diffusion-coefficient method [3, 5] for the turbulent case; and (v) the buoyancy effects can be ignored due to their smallness [6].

The continuity, momentum and energy equations used in the modeling for the laminar plasma jet case can thus be written as follows [3, 5, 6]:

$$\frac{\partial}{\partial x}(\rho u)+\frac{1}{r}\frac{\partial}{\partial r}(r\rho v)=0 \tag{1}$$

$$\frac{\partial(\rho uu)}{\partial x}+\frac{1}{r}\frac{\partial(r\rho uv)}{\partial r}=-\frac{\partial p}{\partial x}+2\frac{\partial}{\partial x}\left(\mu\frac{\partial u}{\partial x}\right)+\frac{1}{r}\frac{\partial}{\partial r}\left[r\mu\left(\frac{\partial u}{\partial r}+\frac{\partial v}{\partial x}\right)\right] \tag{2}$$

$$\frac{\partial(\rho uv)}{\partial x}+\frac{1}{r}\frac{\partial(r\rho vv)}{\partial r}=-\frac{\partial p}{\partial r}+\frac{2}{r}\frac{\partial}{\partial r}\left(r\mu\frac{\partial v}{\partial r}\right)+\frac{\partial}{\partial x}\left[\mu\left(\frac{\partial v}{\partial x}+\frac{\partial u}{\partial r}\right)\right]-2\mu\frac{v}{r^2} \tag{3}$$

$$\begin{aligned}\frac{\partial(\rho uh)}{\partial x}+\frac{1}{r}\frac{\partial(r\rho vh)}{\partial r}&=\frac{\partial}{\partial x}\left[\frac{k}{c_p}\frac{\partial h}{\partial x}\right]+\frac{1}{r}\frac{\partial}{\partial r}\left[r\frac{k}{c_p}\frac{\partial h}{\partial r}\right]-U_r\\&-\frac{\partial}{\partial x}[(h_A-h_B)J_x]-\frac{1}{r}\frac{\partial}{\partial r}[r(h_A-h_B)J_r]\\&-\frac{\partial}{\partial x}\left[\frac{k}{c_p}(h_A-h_B)\frac{\partial f_A}{\partial x}\right]-\frac{1}{r}\frac{\partial}{\partial r}\left[r\frac{k}{c_p}(h_A-h_B)\frac{\partial f_A}{\partial r}\right]\end{aligned} \tag{4}$$

Here u and v are the axial (x-) and radial (r-) velocity components; p the pressure; and ρ, μ, k, c_p, h and U_r are the temperature- and composition-dependent plasma density, viscosity, thermal conductivity, specific heat at constant pressure, specific enthalpy

and radiation power per unit volume, respectively. In Eq. (4), the terms containing $(h_A - h_B)$ represent the contribution of species diffusion to the energy transport, where h_A and h_B are the temperature -dependent specific enthalpies of pure argon and pure air, respectively. f_A is the mass fraction of argon in the argon-air mixture and is solved by use of the following species conservation equation:

$$\frac{\partial(\rho u f_A)}{\partial x}+\frac{1}{r}\frac{\partial(r\rho v f_A)}{\partial r}=\frac{\partial}{\partial x}\left[\Gamma_f\frac{\partial f_A}{\partial x}\right]+\frac{1}{r}\frac{\partial}{\partial r}\left[r\Gamma_f\frac{\partial f_A}{\partial r}\right]+S_f \quad (5)$$

J_x and J_r are axial (x-) and radial (r-) components of the argon diffusion mass flux vector [4]. The transport coefficient in Eq. (5) can be expressed as [6] $\Gamma_f=\left[\overline{m}_A\overline{m}_B/(\overline{M}\overline{M}_A)\right]\rho\,\overline{D}^x_{AB}$, in which $\overline{M}$ and $\overline{M}_A$ are the averaged gas-particle mass for all the gas particles (including electrons) of the gas mixture and that for all the gas particles coming from argon [4], respectively, while $\overline{m}$ and $\overline{m}_A$ are their counterparts only accounting for heavy particles (excluding electrons). The source term S_f in Eq. (5) can be expressed as [6]

$$S_f=\frac{1}{r}\frac{\partial}{\partial r}\left(r\Gamma_f\frac{f_A}{\overline{M}}\frac{\partial\overline{M}}{\partial r}\right)-\frac{1}{r}\frac{\partial}{\partial r}\left(r\Gamma_f\frac{f_A}{\overline{M}_A}\frac{\partial\overline{M}_A}{\partial r}\right)+\frac{\partial}{\partial x}\left(\Gamma_f\frac{f_A}{\overline{M}}\frac{\partial\overline{M}}{\partial x}\right)$$
$$-\frac{\partial}{\partial x}\left(\Gamma_f\frac{f_A}{\overline{M}_A}\frac{\partial\overline{M}_A}{\partial x}\right)+\frac{1}{r}\frac{\partial}{\partial r}\left(r\overline{D}^T_{AB}\frac{\partial\ln T}{\partial r}\right)+\frac{\partial}{\partial x}\left(\overline{D}^T_{AB}\frac{\partial\ln T}{\partial x}\right) \quad (6)$$

$\overline{D}^x_{AB}$ and $\overline{D}^T_{AB}$ are the combined ordinary diffusion coefficient and the combined thermal diffusion coefficient [4].

On the other hand, for the study of the characteristics of turbulent argon plasma jets issuing into ambient air, Eq. (1) — (5) are still be employed but all the physical quantities appearing in those equations are their time-averaged values. In addition, the molecular transport coefficients appearing in Eqs. (2) – (5) are substituted by their counterparts containing both the turbulent and molecular contributions. The K–ε two-equation turbulence model is employed to model the turbulent plasma flow and calculate the turbulent viscosity [3, 5].

The computational domain used in the modeling is denoted as A-B-C-D-E-A in Fig. 1. The radius of the jet inlet (A-B) is 4 mm. D-E is the flat plate impinged by the plasma jet, and the radial size (DE or AC) of the computational domain is taken to be 50 mm. The axial size (CD or AE) can vary in the range of 10 – 100 mm to investigate the effect of the distance between the flat plate and the jet inlet (will be denoted by L and called the plate standoff distance hereafter). Boundary conditions are as follows:

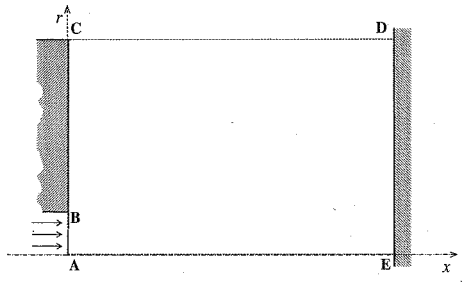

Fig. 1 Computational domain

(i) At the jet inlet (A-B): v = 0, $f_A = 1.0$, and the following profiles of axial velocity and temperature are used:

$$u=U_0[1-(r/R_{in})^{1.4}]$$
$$T=(T_0-T_w)[1-(r/R_{in})^{2.3}]+T_w \quad (7)$$

in which R_{in} is the radius of the jet inlet section (4 mm), T_w is the inner wall temperature of plasma torch and T_w= 700 K, whereas U_0 and T_0 are the maximum axial velocity and temperature at the jet-inlet center, respectively. For the turbulent cases, the turbulent kinetic energy and its dissipation rate at the jet inlet section A-B are given by the same way as in [3, 5].

(ii) At the rear surface B-C of the plasma torch wall, for the laminar case, u = v = 0 and zero diffusion flux are employed, and the wall temperature is assumed to vary in the radial direction according to the relation $T=700-400\ln(r/R_{in})/\ln(R_{out}/R_{in})$, in which R_{out} is the outer radius of the plasma torch (50 mm). For the turbulent jet case, the wall function method is used to treat the B-C boundary conditions.

(iii) Along the top free boundary C-D, the following conditions are employed:

$$\partial u/\partial r=0,\ \partial(\rho rv)/\partial r=0 \quad (8)$$
$$\text{if } v<0:\ T=300\,\text{K},\ f_A=0,\ K=0\ \ \varepsilon=0$$
$$\text{if } v>0:\ \partial T/\partial r=0,\ \partial f_A/\partial r=0,\ \partial K/\partial r=0,\ \partial\varepsilon/\partial r=0$$

(iv) At the plate surface D-E, for the laminar case, u = v = 0 and zero diffusion flux are employed and the wall temperature is assumed to be 1000 K. For the turbulent jet case, the wall function method is also used to treat the D-E boundary conditions.

(v) Along the jet axis A-E, the axi-symmetrical conditions are employed:

$$\partial\phi/\partial r=0\ \ (\phi=u,h,f_A,K,\varepsilon),\ \ v=0 \quad (9)$$

SIMPLE algorithm has been used to solve the governing equations. The number of grid points employed in the computation is 124 (x-) × 78 (r-direction). Non-uniform mesh is adopted with finer mesh spacing near the plate surface and the jet axis.

RESULTS AND DISCUSSION

Typical modeling results are presented in Figs. 2−5 to compare the characteristics of laminar and turbulent argon plasma jets impinging normally upon the flat plate in ambient air. In order to reveal more clearly the difference between the characteristics of laminar and turbulent plasma impinging-jets, the same values of the U_0 and T_0 in the radial profiles (7) will be used for both the laminar and turbulent cases. It is noted that in experiments sometimes both laminar and turbulent plasma jets may be generated under almost the same jet inlet conditions.

Figure 2 compares the computed temperature distributions in laminar (upper semi-plane) and

turbulent (lower semi-plane) plasma impinging-jets for the cases with the same jet-inlet temperature (T_0 = 14000 K) and velocity (U_0 = 1000 m s^{-1}) profiles but different plate standoff distances (10 and 100 mm). It is seen that when the plate standoff distance is comparatively large (e.g. 100 mm), the plasma temperature at the outer edge of stagnation-point boundary layer for the laminar jet is appreciably higher than that for the turbulent jet because larger entrained flow rate of the ambient air and thus rapider decaying rate of plasma temperature are involved in the turbulent plasma jet. However, when the plate standoff distance is as short as 10 mm, the difference between laminar and turbulent plasma impinging-jets in their high-temperature regions is not appreciable due to the presence of the 'potential core' and a recirculating vortex in the turbulent plasma jet.

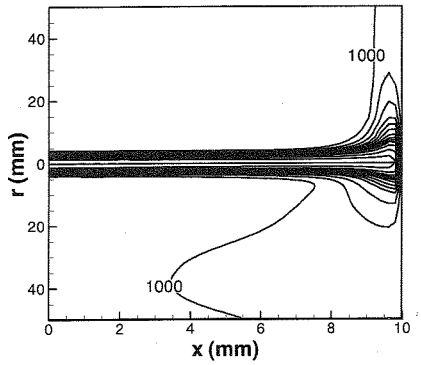

(a) L=10 mm

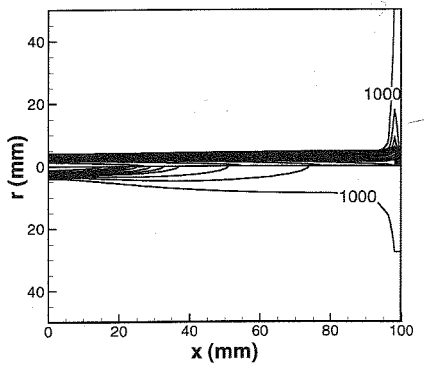

(b) L= 100 mm

Fig.2. Comparison of the computed temperature fields in the laminar (upper semi-plane) and turbulent (lower semi-plane) plasma impinging-jets. Outermost isotherm – 1000 K, isotherm interval – 2000 K

The impinging jet behavior is revealed more clearly in Figs. 3 and 4. Figure 3 plots the variations of plasma temperature along the axes of the laminar (a) and turbulent (b) plasma impinging-jets for a few different plate standoff distances. In this figure, the numerals represent the plate standoff distances, i.e. L = 10, 20, 30 or 40 mm, respectively. Since the unceasing entrainment of ambient air into the plasma jets, the plasma temperature always decreases with increasing axial distance from the jet inlet. Rapider decreases only appear in the region near the plate surface. It

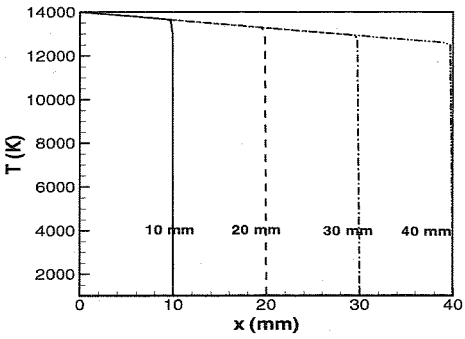

(a) Laminar jets

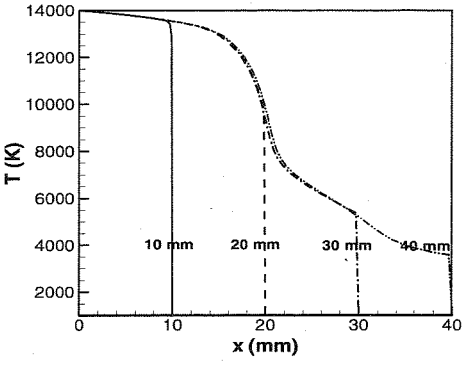

(b) Turbulent jets

Fig.3. Variations of the plasma temperature along the axes of the plasma impinging-jets for different plate standoff distances. T_0 = 14000 K and U_0 =1000 m s^{-1}.

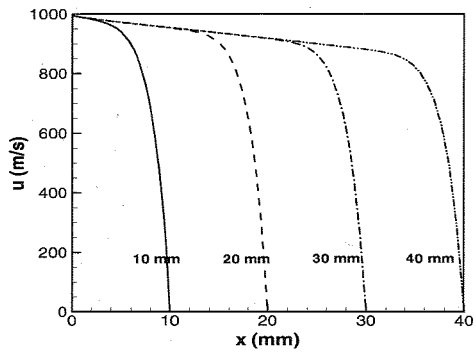

(a) Laminar jets

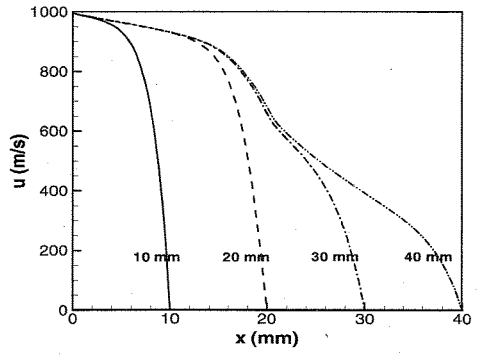

(b) Turbulent jets

Fig.4. Variations of the axial-velocity along the axes of the plasma impinging-jets for different plate standoff distances. T_0 = 14000 K and U_0 =1000 m s^{-1}.

means that the presence of plate only affect appreciably the temperature distributions in the region near the plate. Corresponding predicted results are presented in Fig. 4 concerning the variations of axial velocity along the axes of the laminar (a) and turbulent (b) plasma impinging-jets for the 4 different plate standoff distances. It is also seen that the axial velocity always decreases with increasing axial distance due to the air entrainment, and rapider decreases appear in the region near the plate surface. However, the plate affecting-zones for the velocity distributions are somewhat wider than that for the temperature distributions.

Figure 5 compares axial variations of the mass flow rate of the ambient air entrained into the laminar and turbulent plasma impinging-jets for different plate standoff distances. The computed results of free jets are also presented in Fig. 5(a) and 5(b) in order to compare the entrainment rates of free and impinging plasma jets. It is found that the existence of the flat plate not only forces the forward-flowing main jet change its flow direction but also significantly enhances the mass flow rate of the ambient air entrained into the impinging jet in comparison with the free plasma jet, especially for the laminar case,

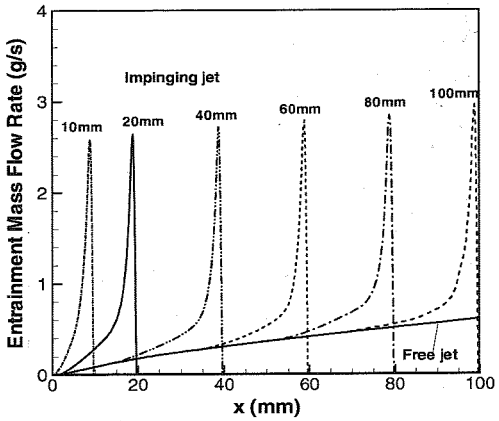

(a) Laminar jets

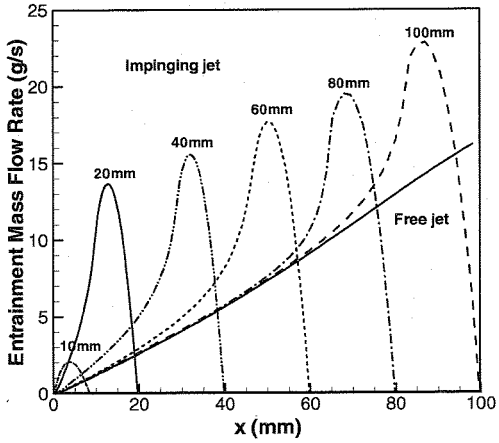

(b) Turbulent jets

Fig.5. Variations of the mass flow rate of air entrained into the plasma jets along the axis of the plasma impinging-jet for different plate standoff distances. T_0 = 14000 K and U_0 =1000 m s^{-1}.

due to the additional entrainment of the wall jet. The maximum mass flow rates of ambient air entrained into the laminar or turbulent plasma impinging-jets increase with increasing plate standoff distance, but the maximum mass flow rates entrained into the laminar free and impinging jet are less than those for the turbulent case.

CONCLUSIONS

Modeling results concerning the characteristics of laminar and turbulent argon plasma jets impinging normally upon a flat plate in ambient air show that due to the additional entrainment produced by the wall jet flowing along the plate surface, the mass flow rate of ambient air entrained into the impinging jet is larger than that into corresponding free jet. The additional entrainment of wall jet is more significant for the laminar plasma impinging -jet. The plasma parameters (temperature, axial velocity, etc.) are affected by the presence of the plate mainly in the near-plate region, and the decaying rates of the plasma parameters in the turbulent impinging jet are often appreciably larger than their laminar counterparts due to that more ambient air is entrained into the turbulent jet.

ACKNOWLEDGMENT

This work was supported by the National Natural Science Foundation of China (grant Nos. 50336010, 10405015, 10575127)

REFERENCES

[1] W. X. Pan, W. Hua Zhang, W. Hong Zhang, C. K. Wu, "Generation of Long, laminar plasma jets at atmospheric pressure and effects of flow turbulence," Plasma Chem. Plasma Process., **21** (2), pp. 23-35, 2001

[2] W.X. Pan, X. Meng, G. Li, Q.X. Fei, C.K. Wu, "Feasibility of laminar plasma-jet hardening of cast iron surface", Surf. Coat. Technol., **197** (2/3), pp. 345 -350, 2005

[3] K. Cheng, Xi Chen, W. X. Pan, "Comparison of laminar and turbulent thermal plasma jet characteristics – a modeling study," to appear in Plasma Chem. Plasma Process. (2006).

[4] A.B. Murphy, "Diffusion in equilibrium mixtures of ionized gases", Phys. Rev. E, **48** (5), pp. 3594-3603, 1993

[5] K. Cheng, Xi Chen, "Prediction of the entrainment of ambient air into a turbulent argon plasma jet using a turbulence-enhanced combined-diffusion-coefficient method", Int. J. Heat Mass Transfer, **47** (23), pp. 5139-5148, 2004

[6] K. Cheng, Xi Chen, "Effects of natural convection on the characteristics of long laminar argon plasma jets issuing upwards or downwards into ambient air — a numerical study", J. Phys. D: Appl. Phys., **37**, (17), pp. 2385-2391, 2004